UNIVERSITY OF COPENHAGEN
NIELS BOHR INSTITUTE

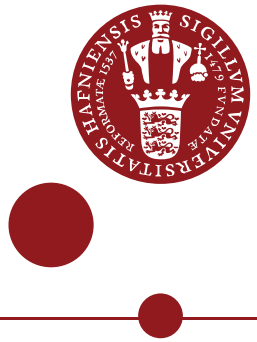

Bachelor thesis

Carl Jordan Eriksen

Exact Diagonalisation of a Triple-Quantum Dot Toy Model

Ferromagnetism in a triangular configuration of quantum dots

Advisor: Michele Burrello

Niels Bohr Institute. June 15, 2022

Abstract

A recent experiment has demonstrated Nagaoka's ferromagnetism in a quantum dot system [3]. This thesis investigates the ferromagnetism of a toy model of a three-site quantum dot system using the Hubbard model and an exact diagonalisation method. Two cases are considered: two-electron filling and four-electron filling. The former is found not to lead to ferromagnetism. The latter, conversely, is found to lead to ferromagnetism in large parts of the four-electron system's phase space. A method is proposed for spin measurements based on a spin-to-charge conversion.

Contents

Chapter 1

Introduction

Theory has long predicted the phenonenon of itinerant magnetism in condensed matter systems—i.e. magnetism caused only by the Coulomb interaction of electrons, which are free to move around in the system [8]. One such example is Nagaoka's ferromagnetism, which in an N-site lattice at a filling of $N-1$ electrons arises in the limit of infinite characteristic energies of the Coulomb interactions between the electrons. Nagaoka proved in the Hubbard model that these conditions lead to the ground state having the electron spins pointing in the same direction and therefore being ferromagnetic [7]. Recently, Nagaoka's ferromagnetism was demonstrated experimentally in a quantum simulation system in the form of a four-site quantum dot plaquette with a filling of three electrons (therefore fulfilling the $N-1$-filling condition) and large interaction energies [3]. Quantum dots are electrostatically defined 'traps' in semiconductor heterostructures which can achieve thermal energies much lower than that of the tunnelling (hopping) amplitudes between dots and the characteristic energies of the Coulomb repulsion for electrons located on the same dot; various geometries of quantum dot arrays therefore provide ideal platforms for quantum simulations of phenomena in strongly-correlated electron systems and quantum computation [6].

In this thesis, the possibility of a quantum simulation of Nagaoka's ferromagnetism in a three-site triangular quantum dot array, as seen in Fig. 2.1, is explored. Both two-electron filling and four-electron (two-hole) filling are considered. Real quantum dot systems are of course subject to a diverse range of effects related to material disorder, fabrication imperfections, and interactions with the environment. These, along with temperature, will be ignored in the toy model approach employed in this thesis, as the goal is to explore coarsely the most important physical phenomena and to gain an indication of the experimental possibilites of the system. In Ch. 2, the model is introduced including naturally the definition of the Hilbert spaces and the Hamiltonian. We use the Hubbard model Hamiltonian along with two terms which give rise to the magnetic Aharonov-Bohm and Zeeman effects. The symmetries of the Hamiltonian and their implications on the analysis are discussed. In Ch. 3, the results for the two-electron and four-electron systems are presented. The spectra in the translationally invariant non-interacting limit are calculated and the Coulomb interaction is treated perturbatively. Then, using exact diagonalisation methods, we numerically determine the energies of the interacting part of the phase space, and a phase diagram is presented in Fig. 3.5 showing that large parts of the phase space of the four-electron system exhibits ferromagnetism. The interplay of the two magnetic effects is also explored. Finally, a protocol for the measurement of the spin of the system is proposed based on an adiabatic detuning scan. Concluding remarks and an experimental outlook are given in Ch. 4.

Chapter 2
Theory

This chapter introduces the model in which the calculations in Ch. 3 are performed. We begin immediately below by defining the two-electron and four-electron Hilbert spaces of the problem, and then in Sec. 2.2 follow by introducing the Hubbard Hamiltonian and the two magnetic effects. To simplify the analysis, we discuss in Sec. 2.3 the important conserved quantites of the Hamiltonian, namely the particle number, the spin and the crystal momentum. Throughout the thesis, we will work in the second quantisation formalism of quantum mechanics. Further background on this is given in Appendix A.

2.1. Hilbert spaces

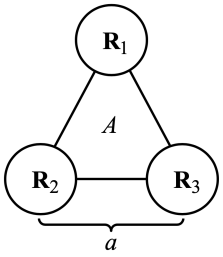

Figure 2.1. Diagrammatic representation of the system.

The three dots are in the triangular configuration depicted in Fig. 2.1, with A being the area of the triangle and a the lattice spacing. The sites of the dots are indexed by $r = 1, 2, 3$, and we imagine them to be potential traps described by the Hamiltonians H_r. The locations of the sites are

$$\mathbf{R}_1 = a\begin{pmatrix} 1/2 \\ \sqrt{3}/2 \end{pmatrix}, \qquad \mathbf{R}_2 = \begin{pmatrix} 0 \\ 0 \end{pmatrix}, \qquad \mathbf{R}_3 = a\begin{pmatrix} 1 \\ 0 \end{pmatrix}, \tag{2.1}$$

and the lattice spacing will be taken to be of order 2×10^2 nm. Each site Hamiltonian H_r admits a set of eigenstates $\{|\psi_{n,r}\rangle\}$ with n being the principal quantum number. For the analysis in this thesis, we will imagine the level spacing between the ground state and first excited state $E_{2,r} - E_{1,r}$ to be so much larger than the other energy scales in the problem, such that orbitals other than $|r\rangle = |\psi_{1,r}\rangle$ can safely be ignored. As the states are to be electron states, a spin degree of freedom must also be included. Taking $\sigma = \uparrow, \downarrow$ to be the z-component of the electron spin, we end up with six orthonormal single-particle orbitals $\{|r\rangle \otimes |\sigma\rangle\}$. We now define the zero-particle vacuum state $|\Omega\rangle$ and the creation and annihilation operators $c^\dagger_{r,\sigma}$ and $c_{r,\sigma}$, which obey the anticommutation relations in Eq. (A.3).

Below we define a basis for the two-particle and the four-particle Hilbert space of this system. As we will see, the Hamiltonian conserves the electron number N and the spin component S_z, making it prudent to choose a basis for which these are well-defined, as this ensures that the representation of the Hamiltonian becomes block-diagonal. The terminology local and non-local combination will be used to signify combinations of particles at the same site or at different sites. E.g. the middle set of states in Eq. (2.2) are non-local.

2.1.1. Two-particle Hilbert space

Taking the r-index to be defined modulo 3 (i.e. $r = 4 \mod 3 = 1$), the basis for the 15-dimensional two-particle Hilbert spaces comprises in part nine triplets

$$\{c^\dagger_{r,\uparrow}c^\dagger_{r+1,\uparrow}|\Omega\rangle\} \cup \left\{\frac{1}{\sqrt{2}}(c^\dagger_{r,\uparrow}c^\dagger_{r+1,\downarrow} + c^\dagger_{r,\downarrow}c^\dagger_{r+1,\uparrow})|\Omega\rangle\right\} \cup \{c^\dagger_{r,\downarrow}c^\dagger_{r+1,\downarrow}|\Omega\rangle\} \quad \text{for } r = 1, 2, 3 \tag{2.2}$$

with $S_z = 1, 0, -1$ from left to right. In addition the basis includes the six singlets

$$\{c^\dagger_{r,\uparrow}c^\dagger_{r,\downarrow}|\Omega\rangle\} \cup \left\{\frac{1}{\sqrt{2}}(c^\dagger_{r,\uparrow}c^\dagger_{r+1,\downarrow} - c^\dagger_{r,\downarrow}c^\dagger_{r+1,\uparrow})|\Omega\rangle\right\} \quad \text{for } r = 1, 2, 3. \tag{2.3}$$

2.1.2. Four-particle Hilbert space

This Hilbert space is also 15-dimensional, and the basis states can in fact be defined in analogy with Eqs. (2.2) and (2.3). We define the totally filled state

$$|\Omega_h\rangle = \prod_{r,\sigma} c^\dagger_{r,\sigma}|\Omega\rangle, \tag{2.4}$$

which might equivalently be interpreted as a hole vacuum. It is then easy to construct the four-electron basis of nine triplets

$$\{c_{r,\uparrow}c_{r+1,\uparrow}|\Omega_h\rangle\} \cup \left\{\frac{1}{\sqrt{2}}(c_{r,\uparrow}c_{r+1,\downarrow} + c_{r,\downarrow}c_{r+1,\uparrow})|\Omega_h\rangle\right\} \cup \{c_{r,\downarrow}c_{r+1,\downarrow}|\Omega_h\rangle\} \quad \text{for } r = 1, 2, 3, \tag{2.5}$$

and six singlets

$$\{c_{r,\uparrow}c_{r,\downarrow}|\Omega_h\rangle\} \cup \left\{\frac{1}{\sqrt{2}}(c_{r,\uparrow}c_{r+1,\downarrow} - c_{r,\downarrow}c_{r+1,\uparrow})|\Omega_h\rangle\right\} \quad \text{for } r = 1, 2, 3. \tag{2.6}$$

In the hole picture, these are then two-hole states.

2.2. Hamiltonian

Systems of highly correlated electrons on a lattice of localised orbitals $\{|i\rangle\}$ are often modelled in the Fermi-Hubbard model, which is described by the Hamiltonian

$$\mathcal{H} = -\sum_{\langle i,j\rangle}\sum_{\sigma} t_{i,j}c^\dagger_{i,\sigma}c_{j,\sigma} + U\sum_i c^\dagger_{i,\uparrow}c_{i,\uparrow}c^\dagger_{i,\downarrow}c_{i,\downarrow}, \tag{2.7}$$

where $\langle i, j\rangle$ denotes a nearest-neighbor sum [1]. The first term $\mathcal{H}_{\text{kin}}$ is analagous to the tight-binding Hamiltonian and models the hopping of an electron from orbitals $|j\rangle$ to $|i\rangle$. The second term $\mathcal{H}_{\text{int}}$ models the Coulomb interaction of different-spin electrons occupying the same orbital $|i\rangle$, as $c^\dagger_{i\uparrow}c_{i\uparrow}c^\dagger_{i\downarrow}c_{i\downarrow} = \hat{n}_{i\uparrow}\hat{n}_{i\downarrow}$ vanishes unless $n_{i\uparrow} = n_{i\downarrow} = 1$. For our purposes, the Hamiltonian may be rewritten and extended in the following way

$$\mathcal{H} = \sum_{r,\sigma}\delta_r\hat{n}_{r,\sigma} - t\sum_{r,\sigma}(c^\dagger_{r+1,\sigma}c_{r,\sigma} + \text{h.c.}) + U\sum_r \hat{n}_{r,\uparrow}\hat{n}_{r,\downarrow}. \tag{2.8}$$

The addition of the first term allows for a difference in the chemical potentials at each site, which we call detunings. The second term is again the hopping term where again the r-index is defined modulo 3 and the hopping parameters $t_{i,j} = t$ are taken to be homogeneous. The on-site interaction may also be written

$$\mathcal{H}_{\text{int}} = \frac{U}{2}\sum_r \hat{N}_r(\hat{N}_r - 1), \tag{2.9}$$

where $\hat{N}_r = \hat{n}_{r,\uparrow} + \hat{n}_{r,\downarrow}$ is the number of electrons occupying the orbital $|r\rangle$.

The effects of a magnetic field $\mathbf{B} = B\hat{\mathbf{z}}$ are two-fold. The first is the Aharonov-Bohm effect—electrons accrue a phase related to the magnetic flux when tunneling between sites. The second is the Zeeman effect—electrons have a magnetic moment which interacts with the field.

2.2.1. Aharonov-Bohm effect

As is usual in quantum mechanics, the effect of the magnetic field $\mathbf{B} = \nabla \times \mathbf{A}$ on a system described by the Schrödinger equation

$$H(\mathbf{p}, \mathbf{r})\Psi = i\hbar\dot{\Psi} \tag{2.10}$$

is taken into account through the minimal coupling Hamiltonian, which is obtained by the substitution

$$H(\mathbf{p}, \mathbf{r}) \mapsto H(\mathbf{p} - q\mathbf{A}, \mathbf{r}). \tag{2.11}$$

Here, q is the charge of the particle [4]. Equivalently, the wavefunction may be transformed by the gauge transformation

$$\Psi' = e^{i\theta(\mathbf{r})}\Psi, \qquad \theta(\mathbf{r}) = \frac{q}{\hbar}\int_{\mathbf{r}_0}^{\mathbf{r}} \mathrm{d}\mathbf{r}' \cdot \mathbf{A}(\mathbf{r}'), \tag{2.12}$$

where $\mathbf{r}_0$ is an arbitrary reference point. This wavefunction will satisfy the Schrödinger equation in Eq. (2.10). The same gauge transformation can also be performed in second quantisation, where it is called the Peierls substitution. It is effected by the transformation

$$c_{r,\sigma} \mapsto e^{i\theta(\mathbf{R}_r)}c_{r,\sigma}, \qquad c^\dagger_{r,\sigma} \mapsto e^{-i\theta(\mathbf{R}_r)}c^\dagger_{r,\sigma}; \qquad \theta(\mathbf{R}_r) = \frac{e}{\hbar}\int_{\mathbf{r}_0}^{\mathbf{R}_r} \mathrm{d}\mathbf{r} \cdot \mathbf{A}(\mathbf{r}), \tag{2.13}$$

where we have let $q = -e$ [5]. The hopping terms in Eq. 2.20 are the only affected terms, and they transform in the following way

$$-tc^\dagger_{r+1,\sigma}c_{r,\sigma} \mapsto -te^{-i\left(\theta(\mathbf{R}_{r+1})-\theta(\mathbf{R}_r)\right)}c^\dagger_{r+1,\sigma}c_{r,\sigma}, \tag{2.14}$$

where the Peierls phase is then defined as

$$\theta^p_r = \theta(\mathbf{R}_{r+1}) - \theta(\mathbf{R}_r) = \frac{e}{\hbar}\int_{\mathbf{R}_r}^{\mathbf{R}_{r+1}} \mathrm{d}\mathbf{r} \cdot \mathbf{A}(\mathbf{r}). \tag{2.15}$$

This phase is related to the magnetic flux, which can be seen by considering the translation of the state $c^\dagger_{1\sigma}|\Omega\rangle$ around the triangle

$$e^{-i\theta^p_3}e^{-i\theta^p_2}e^{-i\theta^p_1}c^\dagger_{1,\sigma}c_{3,\sigma}c^\dagger_{3,\sigma}c_{2,\sigma}c^\dagger_{2,\sigma}c_{1,\sigma}c^\dagger_{1,\sigma}|\Omega\rangle = e^{-i(\theta^p_3+\theta^p_2+\theta^p_1)}c^\dagger_{1,\sigma}|\Omega\rangle. \tag{2.16}$$

The accumulated phase is then

$$\begin{aligned}\theta^p_3 + \theta^p_2 + \theta^p_1 &= \frac{e}{\hbar}\oint_{\partial\mathcal{T}} \mathrm{d}\mathbf{r} \cdot \mathbf{A}(\mathbf{r}) \\ &= \frac{e}{\hbar}\int_{\mathcal{T}} \mathrm{d}^2\mathbf{r} \cdot \mathbf{B}(\mathbf{r}) \\ &= \frac{e\Phi}{\hbar} \\ &= \frac{2\pi\Phi}{\Phi_0},\end{aligned} \tag{2.17}$$

where $\mathcal{T}$ (resp. $\partial\mathcal{T}$) is the surface (resp. boundary) of the triangle, and $\Phi_0 = h/e$ is the flux quantum. The Peierls phase can thus be taken to be $\theta^p_r = 2\pi\Phi/3\Phi_0$ for all r, and the substitution amounts to replacing the tunnelling terms of the Hamiltonian with

$$-te^{-i2\pi\Phi/3\Phi_0}c^\dagger_{r+1,\sigma}c_{r,\sigma}. \tag{2.18}$$

It should be noted that the above is based on the approximation of the dots being pointlike and located at $\mathbf{R}_r$. More sophisticated approaches would involve averaging over the wavefunctions $|r\rangle$, but that is beyond the scope of this thesis.

2.2.2. Zeeman effect

The interaction of the magnetic field with the electronic magnetic dipoles is described by the Zeeman term

$$\begin{aligned}\mathcal{H}_Z &= g\mu_B B S_z \\ &= \frac{1}{2} g\mu_B B \sum_r c_r^\dagger \sigma_z c_r \\ &= \frac{1}{2} g\mu_B B \sum_r (c_{r,\uparrow}^\dagger c_{r,\uparrow} - c_{r,\downarrow}^\dagger c_{r,\downarrow}),\end{aligned} \tag{2.19}$$

where the definition of the spin operator is given in Sec. 2.3.2 and μ_B is the Bohr magneton. The effective Landé factor in GaAs is $g = -0.44$ [9].

The complete Hamiltonian of the model is thus

$$\mathcal{H} = \sum_{r,\sigma} \delta_r \hat{n}_{r,\sigma} - t \sum_{r,\sigma} (e^{-i2\pi\Phi/3\Phi_0} c_{r+1,\sigma}^\dagger c_{r,\sigma} + \text{h.c.}) + U \sum_r \hat{n}_{r,\uparrow}\hat{n}_{r,\downarrow} + \frac{1}{2} g\mu_B B \sum_r c_r^\dagger \sigma_z c_r \tag{2.20}$$

2.3. Symmetries and conserved quantities

The Hamiltonian in Eq. (2.20) has several symmetries, which, as mentioned in Sec. 2.1, will simplify the analysis. From elementary quantum mechanics, we know that if a certain observable $\hat{O}$ representing a generator of a symmetry satisfies $[\mathcal{H}, \hat{O}] = 0$, then the eigenvalues of $\hat{O}$ are conserved, and we may choose a simultaneous eigenbasis for $\mathcal{H}$ and $\hat{O}$. This ensures that $\mathcal{H}$ is block-diagonal, with each block associated with a degenerate eigenspace of $\hat{O}$.

2.3.1. Particle number

We wish to show that N is a conserved quantity, i.e. $[\mathcal{H}, \hat{N}] = 0$. Start by noting that the commutator is linear, and that we have the identity

$$[\hat{n}_{r\uparrow}\hat{n}_{r\downarrow}, \hat{N}] = [\hat{n}_{r\uparrow}, \hat{N}]\hat{n}_{r\downarrow} + \hat{n}_{r\uparrow}[\hat{n}_{r\downarrow}, \hat{N}]. \tag{2.21}$$

Due to the preceding two observations, it is enough to consider the commutator $[c_{r_1,\sigma_1}^\dagger c_{r_2,\sigma_2}, \hat{N}]$ for any (r_1, σ_1) and (r_2, σ_2). We expand

$$[c_{r_1,\sigma_1}^\dagger c_{r_2,\sigma_2}, \hat{N}] = \sum_{r,\sigma} \left(c_{r_1,\sigma_1}^\dagger c_{r_2,\sigma_2} c_{r,\sigma}^\dagger c_{r,\sigma} - c_{r,\sigma}^\dagger c_{r,\sigma} c_{r_1,\sigma_1}^\dagger c_{r_2,\sigma_2} \right). \tag{2.22}$$

From the anticommutation relations in Eq. (A.3) it follows for any (r', r) and (σ', σ) that

$$c_{r',\sigma'} c_{r,\sigma}^\dagger = \delta_{r',r}\delta_{\sigma',\sigma} - c_{r,\sigma}^\dagger c_{r',\sigma'} \tag{2.23}$$

Plugging this into Eq. (2.22) yields

$$[c_{r_1,\sigma_1}^\dagger c_{r_2,\sigma_2}, \hat{N}] = \sum_{r,\sigma} \left(c_{r_1,\sigma_1}^\dagger (\delta_{r_2,r}\delta_{\sigma_2,\sigma} - c_{r,\sigma}^\dagger c_{r_2,\sigma_2}) c_{r,\sigma} - c_{r,\sigma}^\dagger (\delta_{r_1,r}\delta_{\sigma_1,\sigma} - c_{r_1,\sigma_1}^\dagger c_{r,\sigma}) c_{r_2,\sigma_2} \right). \tag{2.24}$$

The Kronecker delta-terms will cancel when summing, leaving us with

$$\begin{aligned}[c_{r_1,\sigma_1}^\dagger c_{r_2,\sigma_2}, \hat{N}] &= \sum_{r,\sigma} \left(c_{r,\sigma}^\dagger c_{r_1,\sigma_1}^\dagger c_{r,\sigma} c_{r_2,\sigma_2} - c_{r_1,\sigma_1}^\dagger c_{r,\sigma}^\dagger c_{r_2,\sigma_2} c_{r,\sigma} \right) \\ &= 0.\end{aligned} \tag{2.25}$$

The particle number is conserved, making the Hamiltonian a direct sum of blocks associated with fixed-particle number subspaces, which justifies the definition of the two-particle and four-particle bases above.

2.3.2. Spin

The spin at site $r = 1, 2, 3$ in the direction $i = x, y, z$ can be measured by applying the operator

$$\hat{S}_{i,r} = \frac{1}{2} c_r^\dagger \sigma_i c_r, \tag{2.26}$$

where σ_i are the Pauli matrices. The total spin of the system in the direction i is then given by

$$\hat{S}_i = \sum_r \hat{S}_{i,r}. \tag{2.27}$$

The spin operators are the generators of spin rotations, so the unitary operator associated with a rotation of the spin at site r about the direction and by the angle defined respectively by $\boldsymbol{\alpha}$ and $\alpha = \|\boldsymbol{\alpha}\|$ is given by

$$\Theta_{\boldsymbol{\alpha},r} = \exp\left[i \sum_j \alpha_j \hat{S}_{j,r} \right] = e^{i\boldsymbol{\alpha}\cdot\hat{\mathbf{S}}_r}, \tag{2.28}$$

and a homogeneous rotation of all the spins is thus associated with the unitary operator

$$\begin{aligned} \Theta_{\boldsymbol{\alpha}} &= \prod_r \Theta_{\boldsymbol{\alpha},r} \\ &= \exp\left[i \sum_r \sum_j \alpha_j \hat{S}_{j,r} \right] \\ &= \exp\left[i \sum_j \alpha_j \hat{S}_j \right] \\ &= e^{i\boldsymbol{\alpha}\cdot\hat{\mathbf{S}}}. \end{aligned} \tag{2.29}$$

If the Hamiltonian commutes with all rotations $\Theta_{\boldsymbol{\alpha}}$, it commutes with the generators of these rotations (see Appendix B). Therefore, commutation with Θ_α for any $\boldsymbol{\alpha}$ implies commutation with all three spin components. For vanishing magnetic field, the Hamiltonian consists solely of sums and products of terms of the form $c_r^\dagger c_{r'}$. In Appendix B it is derived that

$$\Theta_{\boldsymbol{\alpha}} c_r \Theta_{\boldsymbol{\alpha}}^\dagger = U c_r = \exp\left[i \sum_j \frac{\alpha_j}{2} \sigma_j \right] c_r, \tag{2.30}$$

where $U \in \mathrm{SU}(2)$. Thus, for the product $c_r^\dagger c_{r'}$ we obtain

$$\begin{aligned} c_r^\dagger c_{r'} &\mapsto \Theta_{\boldsymbol{\alpha}} c_r^\dagger c_{r'} \Theta_{\boldsymbol{\alpha}}^\dagger \\ &= \Theta_{\boldsymbol{\alpha}} c_r^\dagger \Theta_{\boldsymbol{\alpha}}^\dagger \Theta_{\boldsymbol{\alpha}} c_{r'} \Theta_{\boldsymbol{\alpha}}^\dagger \\ &= c_r^\dagger U^\dagger U c_{r'} \\ &= c_r^\dagger c_{r'}. \end{aligned} \tag{2.31}$$

This implies that $[\Theta_{\boldsymbol{\alpha}}, \mathcal{H}] = 0$, and so the Hamiltonian for vanishing magnetic field conserves all spin components. A finite magnetic field, on the other hand, entails the consideration of the Zeeman Hamiltonian in Eq. (2.19), which consists of terms of the form $c_r^\dagger \sigma_z c_r$. These terms break the rotational invariance about the x-axis and y-axis and consequently do not conserve S_x and S_y. This stems from

$$\begin{aligned} c_r^\dagger \sigma_z c_{r'} &\mapsto \Theta_{\boldsymbol{\alpha}} c_r^\dagger \sigma_z c_r \Theta_{\boldsymbol{\alpha}}^\dagger \\ &= \Theta_{\boldsymbol{\alpha}} c_r^\dagger \Theta_{\boldsymbol{\alpha}}^\dagger \Theta_{\boldsymbol{\alpha}} \sigma_z c_r \Theta_{\boldsymbol{\alpha}}^\dagger \\ &\overset{(*)}{=} c_r^\dagger U^\dagger U \sigma_z c_r \\ &= c_r^\dagger \sigma_z c_r, \end{aligned} \tag{2.32}$$

where the equality $(*)$ is true only if $\boldsymbol{\alpha} \propto \hat{\mathbf{z}}$. Intuitively, this makes sense; if a rotation about e.g. the y-axis is performed on the quantity $\sigma_z c_r$, it must become a linear combination of $\sigma_z c_r$ and $\sigma_x c_r$. In conclusion, the full Hamiltonian in Eq. (2.20) conserves the z-component of spin. As $\hat{S}_z$ and $\hat{\mathbf{S}}^2$ admit a simultaneous eigenbasis, this justifies the definition of the bases in Sec. 2.1 as sets of triplets and singlets.

2.3.3. Crystal momentum

Letting the detunings $\delta_r = 0$ for all r leads to the Hamiltonian being invariant under the transformation $r \mapsto r + 1$ and thus displaying a discrete translational invariance. The Bloch theorem implies in this case that the wavefunctions will be characterised by a crystal momentum k, which is conserved. The crystal momenta for the triangular configuration are $k = 2\pi n/3a$ for $n = 0, 1, 2$.

The Hamiltonian is in fact invariant both under the transformations $r \mapsto r + 1$—which may be regarded as rotations of integer multiples of $2\pi/3$—and reflections about the bisectors of the triangle. These transformations constitute the point group D_3.

Chapter 3
Results

This chapter starts off with an analytical treatment of the non-interacting and translationally invariant limit $U = 0$ and $\delta_r = 0$ for all r. A derivation of the first order singlet-triplet splitting in the four-electron system is presented in Sec. 3.1.1, and it will beckon further investigation of the ferromagnetic properties of this system. In Sec. 3.2, the Hamiltonian is represented in the bases defined in Sec. 2.1, and exact diagonalisation methods are then used in a numerical analysis of the systems. In Sec. 3.3 we find no ferromagnetism in the two-electron system, but in Sec. 3.4, the four-electron system is found to exhibit ferromagnetism in a large region of its phase space. The Aharonov-Bohm and Zeeman effects are investigated numerically in Sec. 3.4.3, and we end in Secs. 3.4.4 and 3.4.5 by proposing a protocol for the measurement of the spin of the system.

3.1. Non-interacting limit

The non-interacting limit is obtained by letting $U = 0$. This makes the Hamiltonian quadratic in the fermionic operators, which affords a simpler treatment of the problem; it suffices to diagonalise the Hamiltonian in a single-particle basis $\{c^\dagger_{r,\sigma}|\Omega\rangle\}$. Defining the vector $\mathbf{C} = (\{c_{r,\sigma}\})^T$ allows the Hamiltonian for $U = 0$ to be expressed

$$\mathcal{H} = \mathbf{C}^\dagger H_{\text{sp}} \mathbf{C}, \tag{3.1}$$

due exactly to its quadratic nature. The single-particle representation of the Hamiltonian H_{sp} can be readily diagonalised by a unitary transformation

$$\mathbf{C}^\dagger H'_{\text{sp}} \mathbf{C} = \mathbf{C}^\dagger U^\dagger H_{\text{sp}} U \mathbf{C}, \tag{3.2}$$

which may of course equivalently be stated as a unitary transformation of the fermionic vector operators

$$\mathbf{D} = (\{d_\nu\})^T = U\mathbf{C}, \tag{3.3}$$

where the fermionic operators $\{d_\nu\}$ annihilate single-particle eigenstates of the Hamiltonian. Many-particle states are then easily constructed simply by populating these states.

We would like to find the unitary transformation U which performs this diagonlisation, and by letting the detunings $\delta_r = 0$, for all r we know based on Sec. 2.3.3 that the Hamiltonian is diagonalised exactly by Fourier transforming the fermionic operators from real space to momentum space—i.e. $\{d_\nu\} = \{\tilde{c}_{k,\sigma}\}$ with $k = 2\pi n/3a$ for $n = 0, 1, 2$. The transformation may be expressed

$$c_{r,\sigma} = \sum_k U_{r,k} \tilde{c}_{k,\sigma} = \frac{1}{\sqrt{3}} \sum_k e^{ikra} \tilde{c}_{k,\sigma} \tag{3.4}$$

We substitute first into the hopping part of the Hamiltonian $\mathcal{H}_{\text{kin}}$, getting

$$\mathcal{H}_{\text{kin}} = -\frac{t}{3} \sum_{r,\sigma} \sum_{k,k'} (e^{-i2\pi\Phi/3\Phi_0} e^{-ik(r+1)a} e^{ik'ra} \tilde{c}^\dagger_{k,\sigma} \tilde{c}_{k',\sigma} + \text{h.c.})$$

$$= -t \sum_{k,k',\sigma} \Big(\Big[\frac{1}{3} \sum_r e^{i2\pi r(n'-n)/3} \Big] e^{-i2\pi\Phi/3\Phi_0} e^{-ika} \tilde{c}^\dagger_{k,\sigma} \tilde{c}_{k',\sigma} + \text{h.c.} \Big). \tag{3.5}$$

The factor in the bracket is exactly $\delta_{k,k'}$, making the sum

$$\begin{aligned} \mathcal{H}_{\text{kin}} &= -t \sum_{k,\sigma} (e^{-ika - i2\pi\Phi/3\Phi_0} \tilde{c}^\dagger_{k,\sigma} \tilde{c}_{k,\sigma} + \text{h.c.}) \\ &= -2t \sum_{k,\sigma} \cos\left(ka + \frac{2\pi\Phi}{3\Phi_0} \right) \tilde{c}^\dagger_{k\sigma} \tilde{c}_{k\sigma}, \end{aligned} \tag{3.6}$$

We thus recover the expected cosine dispersion of the tight-binding model, with an Aharonov-Bohm phase. The Zeeman term $\mathcal{H}_Z$ can also be transformed, giving

$$\begin{aligned} \mathcal{H}_Z &= \frac{1}{6} g\mu_B B \sum_r \sum_{k,k'} e^{-ikra} e^{ik'ra} \tilde{c}^\dagger_k \sigma_z \tilde{c}_{k'} \\ &= \frac{1}{6} g\mu_B B \sum_{k,k'} \sum_r e^{i2\pi r(n'-n)/3} \tilde{c}^\dagger_k \sigma_z \tilde{c}_{k'} \\ &= \frac{1}{2} g\mu_B B \sum_k \tilde{c}^\dagger_k \sigma_z \tilde{c}_k. \\ &= \frac{g\mu_B \Phi}{2A} \sum_k \tilde{c}^\dagger_k \sigma_z \tilde{c}_k \end{aligned} \tag{3.7}$$

The case of no magnetic field and the dispersion in Eq. (3.6) leads to the spectrum depicted in Fig. 3.1a. The two spin-degenerate states of energy $-2t$ have a crystal momentum of $k_0 = 0$, and the spin and momentum degenerate states of energy t have crystal momenta $k_1 = 2\pi/3$ and $k_2 = 4\pi/3$. Turning on a magnetic field has two separate effects as discussed in Secs. 2.2.1 and 2.2.2. Eq. (3.6) shows that the Aharonov-Bohm effect breaks the crystal momentum degeneracy and leads to a spectrum like the one in Fig. 3.1b, where the Zeeman effect has been ignored. Looking at Eq. (3.7), it is clear that the Zeeman effect as usual breaks the spin degeneracy and, ignoring the Aharonov-Bohm effect, leads to a spectrum as in Fig. 3.1c.

The above lets us say some things about the two- and four-electron systems. The two-electron ground state is a singlet, and has an energy of $-4t$. The lowest triplet energy is $-t$ and is six-fold degenerate. On the contrary, the four-electron ground state is six-fold degenerate, with three triplet states and three singlet states. Defining $|\tilde{\Omega}_h\rangle$ analogously to Eq. (2.4), they are

$$\begin{aligned} |T_1\rangle &= \tilde{c}_{k_1,\uparrow} \tilde{c}_{k_2,\uparrow} |\tilde{\Omega}_h\rangle, \\ |T_2\rangle &= \tilde{c}_{k_1,\downarrow} \tilde{c}_{k_2,\downarrow} |\tilde{\Omega}_h\rangle, \\ |T_3\rangle &= \frac{1}{\sqrt{2}} (\tilde{c}_{k_1,\uparrow} \tilde{c}_{k_2,\downarrow} + \tilde{c}_{k_1,\downarrow} \tilde{c}_{k_2,\uparrow}) |\tilde{\Omega}_h\rangle; \end{aligned} \tag{3.8}$$

and

$$\begin{aligned} |S_1\rangle &= \tilde{c}_{k_2,\uparrow} \tilde{c}_{k_2,\downarrow} |\tilde{\Omega}_h\rangle, \\ |S_2\rangle &= \tilde{c}_{k_3,\uparrow} \tilde{c}_{k_3,\downarrow} |\tilde{\Omega}_h\rangle, \\ |S_3\rangle &= \frac{1}{\sqrt{2}} (\tilde{c}_{k_1,\uparrow} \tilde{c}_{k_2,\downarrow} - \tilde{c}_{k_1,\downarrow} \tilde{c}_{k_2,\uparrow}) |\tilde{\Omega}_h\rangle. \end{aligned} \tag{3.9}$$

This degeneracy between triplets and singlets is the first indication that the four-electron system might exhibit more interesting ferromagnetic behaviour.

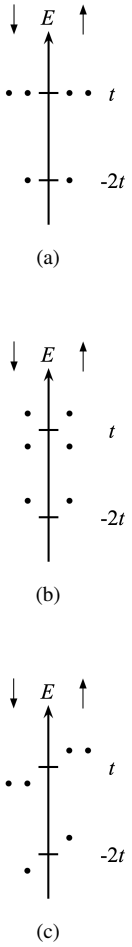

Figure 3.1. Single-particle spectra, with dots representing states.

3.1.1. Perturbative treatment of the on-site interaction

Finding the singlet-triplet splitting in the four-electron system in first order perturbation theory would greatly illuminate whether or not the ground state possesses ferromagnetic properties. The first step in

such a calculation is to transform the on-site interaction from the real space basis into the momentum basis using the transformation in Eq. (3.4),

$$\begin{aligned}\mathcal{H}_{\text{int}} &= U \sum_r c^\dagger_{r,\uparrow} c_{r,\uparrow} c^\dagger_{r,\downarrow} c_{r,\downarrow} \\ &= \frac{U}{9} \sum_{\{k_i\}} \sum_r e^{-ik_1 ra} e^{ik_2 ra} e^{-ik_3 ra} e^{ik_4 ra} c^\dagger_{k_1,\uparrow} c_{k_2,\uparrow} c^\dagger_{k_3,\downarrow} c_{k_4,\downarrow} \\ &= \frac{U}{3} \sum_{\{k_i\}} \left[\frac{1}{3} \sum_r e^{i(k_2+k_4-k_1-k_3)ra} \right] c^\dagger_{k_1,\uparrow} c_{k_2,\uparrow} c^\dagger_{k_3,\downarrow} c_{k_4,\downarrow}. \end{aligned} \tag{3.10}$$

The factor in the brackets is expressing the conservation of momentum in the interaction, $k_2 + k_4 = k_1 + k_3$. Let the momentum transfer $q = k_4 - k_3$. Then

$$\frac{1}{3} \sum_r e^{i(k_2+k_4-k_1-k_3)ra} = \delta_{k_2-k_1,q}, \tag{3.11}$$

which on identifying $k = k_2$ and $k' = k_4$ makes the Hamiltonian

$$\mathcal{H}_{\text{int}} = \frac{U}{3} \sum_{k,k',q} c^\dagger_{k+q,\uparrow} c_{k,\uparrow} c^\dagger_{k'-q,\downarrow} c_{k',\downarrow}. \tag{3.12}$$

We know from Sec. 2.3 that $\mathcal{H}_{\text{int}}$ commutes with the spin operators, meaning that they have simultaneous eigenstates. We need therefore not use degenerate perturbation theory for the triplet subspace. It is also apparant that $\mathcal{H}_{\text{int}}$ conserves the crystal momentum, and as the three singlet states in Eq. (3.9) have different momenta (resp. k_1, k_2, and 0), refraining from degenerate perturbation theory for the singlet subspace is also possible. We start with the first two states in Eq. (3.8), for which

$$\langle T_1 | \mathcal{H}_{\text{int}} | T_1 \rangle = \langle T_2 | \mathcal{H}_{\text{int}} | T_2 \rangle = U, \tag{3.13}$$

as only three terms with $q = 0$ from the sum in Eq. (3.12) contribute. For the third, non-local state, four terms with $q = 0$ contribute, but two terms with $q = k_1$ and $q = k_2$ combine to cancel this fourth zero momentum transfer contribution. Thus,

$$\langle T_3 | \mathcal{H}_{\text{int}} | T_3 \rangle = U. \tag{3.14}$$

For the first two states in Eq. (3.9), we obtain

$$\langle S_1 | \mathcal{H}_{\text{int}} | S_1 \rangle = \langle S_2 | \mathcal{H}_{\text{int}} | S_2 \rangle = \frac{4U}{3}, \tag{3.15}$$

as now four terms with $q = 0$ contribute to the matrix element. The non-local singlet state yields

$$\langle S_3 | \mathcal{H}_{\text{int}} | S_3 \rangle = \frac{5U}{3}, \tag{3.16}$$

because the aforementioned combination of non-zero momentum transfer terms now combine such that they contribute to the sum. The singlet-triplet energy splitting is then

$$\Delta E = \frac{5U}{3} - U = \frac{U}{3}, \tag{3.17}$$

meaning that, at least for small U, one would expect ferromagnetism to occur.

For further investigation of the two-electron and four-electron systems, we must turn to an exact diagonalisation approach, which starts with representing the Hamiltonian in the multiple-particle bases.

3.2. Representations of the Hamiltonian

As discussed in the definition of the Hilbert space in Sec. 2.1, the bases were chosen such as to make the representations block diagonal, with blocks corresponding to well-defined particle number and spin. The two-electron Hilbert space is spanned by the states defined in Eqs. (2.2) and (2.3), and a calculation yields the triplet blocks

$$\mathcal{H}_{N=2}^{S=1,S_z} = \begin{pmatrix} KS_z & e^{i2\pi\Phi/3\Phi_0}t & e^{-i2\pi\Phi/3\Phi_0}t \\ e^{-i2\pi\Phi/3\Phi_0}t^* & \delta + KS_z & e^{i2\pi\Phi/3\Phi_0}t \\ e^{i2\pi\Phi/3\Phi_0}t^* & e^{-i2\pi\Phi/3\Phi_0}t* & \delta + KS_z \end{pmatrix}, \tag{3.18}$$

where $K = g\mu_B B = g\mu_B \Phi/A$ characterises the strength of the Zeeman effect and $S_z = -1, 0, 1$. The singlet block has the form

$$\mathcal{H}_{N=2}^{S=0} = \begin{pmatrix} \mathcal{H}_{N=2}^{\text{l}} & T_{N=2} \\ T_{N=2}^{\dagger} & \mathcal{H}_{N=2}^{\text{n-l}} \end{pmatrix}, \tag{3.19}$$

where the local singlet block is

$$\mathcal{H}_{N=2}^{\text{l}} = \begin{pmatrix} U & 0 & 0 \\ 0 & U & 0 \\ 0 & 0 & 2\delta + U \end{pmatrix};$$

the non-local singlet block is

$$\mathcal{H}_{N=2}^{\text{n-l}} = \begin{pmatrix} 0 & -e^{i2\pi\Phi/3\Phi_0}t & -e^{-i2\pi\Phi/3\Phi_0}t \\ -e^{-i2\pi\Phi/3\Phi_0}t^* & \delta & -e^{i2\pi\Phi/3\Phi_0}t \\ -e^{i2\pi\Phi/3\Phi_0}t^* & -e^{-i2\pi\Phi/3\Phi_0}t^* & \delta \end{pmatrix}; \tag{3.20}$$

and the tunneling block is

$$T_{N=2} = -\sqrt{2}t \begin{pmatrix} e^{-i2\pi\Phi/3\Phi_0} & 0 & e^{i2\pi\Phi/3\Phi_0} \\ e^{i2\pi\Phi/3\Phi_0} & e^{-i2\pi\Phi/3\Phi_0} & 0 \\ 0 & e^{i2\pi\Phi/3\Phi_0} & e^{-i2\pi\Phi/3\Phi_0} \end{pmatrix}. \tag{3.21}$$

The four-electron Hilbert space is spanned by the states in Eqs. (2.5) and (2.6). The triplet blocks are

$$\mathcal{H}_{N=4}^{S=1,S_z} = \begin{pmatrix} 2\delta + U + KS_z & -e^{i2\pi\Phi/3\Phi_0}t & e^{-i2\pi\Phi/3\Phi_0}t \\ -e^{-i2\pi\Phi/3\Phi_0}t^* & \delta + U + KS_z & e^{i2\pi\Phi/3\Phi_0}t \\ e^{i2\pi\Phi/3\Phi_0}t^* & e^{-i2\pi\Phi/3\Phi_0}t^* & \delta + U + KS_z \end{pmatrix}, \tag{3.22}$$

where again $K = g\mu_B B = g\mu_B \Phi/A$ and $S_z = -1, 0, 1$. The singlet block can be written

$$\mathcal{H}^{S=0} = \begin{pmatrix} \mathcal{H}_{N=4}^{\text{l}} & T_{N=4} \\ T_{N=4}^{\dagger} & \mathcal{H}_{N=4}^{\text{n-l}} \end{pmatrix}, \tag{3.23}$$

where

$$\mathcal{H}_{N=4}^{\text{l}} = \begin{pmatrix} 2\delta + 2U & 0 & 0 \\ 0 & 2\delta + 2U & 0 \\ 0 & 0 & 2U \end{pmatrix} \tag{3.24}$$

is the block associated with local states,

$$\mathcal{H}_{N=4}^{\text{n-l}} = \begin{pmatrix} 2\delta + U & e^{i2\pi\Phi/3\Phi_0}t & e^{-i2\pi\Phi/3\Phi_0}t \\ e^{-i2\pi\Phi/3\Phi_0}t^* & \delta + U & e^{i2\pi\Phi/3\Phi_0}t \\ e^{i2\pi\Phi/3\Phi_0}t^* & e^{-i2\pi\Phi/3\Phi_0}t^* & \delta + U \end{pmatrix}, \tag{3.25}$$

is associated with non-local states, and

$$T_{N=4} = \sqrt{2}t \begin{pmatrix} e^{-i2\pi\Phi/3\Phi_0} & 0 & e^{i2\pi\Phi/3\Phi_0} \\ e^{i2\pi\Phi/3\Phi_0} & e^{-i2\pi\Phi/3\Phi_0} & 0 \\ 0 & e^{i2\pi\Phi/3\Phi_0} & e^{-i2\pi\Phi/3\Phi_0} \end{pmatrix} \tag{3.26}$$

represents the tunnelling between these subspaces.

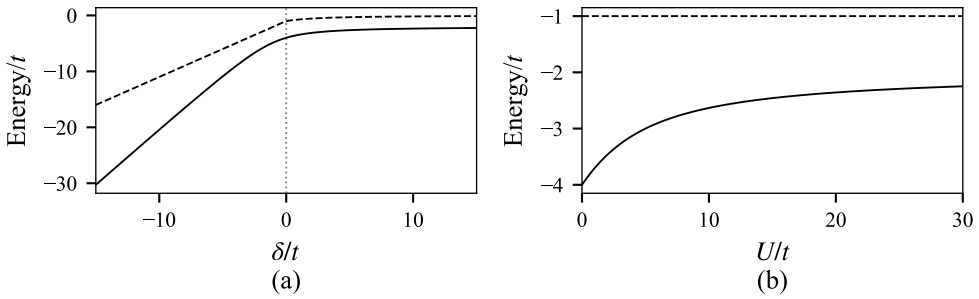

Figure 3.2. Lowest triplet (dashed) and singlet (solid) energies of the two-electron system. (a) Produced with $U = \Phi = 0$. (b) Produced with $\delta = \Phi = 0$.

3.3. Two-electron results

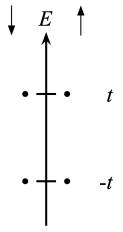

Figure 3.3. Single-particle spectrum for the double-QD system.

The two-electron system is found to be ferromagnetically uninteresting, i.e. the ground state is a singlet at all values of U/t and δ/t. By some heuristic arguments together with the above established fact that the system exhibited a $-4t$ singlet-triplet splitting in the translationally invariant non-interacting limit, this conclusion can be quite easily arrived at by considering some limits. Let $\Phi = 0$ in all cases. Consider first the cases $U = 0$ and $\delta/t \ll -1$. Here, we are effectively dealing with a single-dot system, meaning that the ground state must be a singlet. The opposite limit, $\delta/t \gg 1$, leads again to an effective reduction, but in this case to a double-dot system. The double-dot is just the familiar two-level problem, whose spectrum is displayed in Fig. 3.3 (see e.g. Ch. 6 in [8]). From the spectrum, it is clear that the ground state is a singlet, with the singlet-triplet splitting being $-2t$.

Consider now $\delta = 0$ and $U/t \gg 1$. In this case, it is clear to see that the local singlets will effectively be excluded from the Hilbert space, leaving only the non-local singlets and the triplets. Based on the representations found in the previous section, we may argue that $\mathcal{H}^{\mathrm{l}}_{N=2}$ becomes irrelevant to ground state considerations in the limit, and as the lowest eigenvalue of $\mathcal{H}^{\text{n-l}}_{N=2}$ is $-2t$, the singlet-triplet splitting should, in the large on-site interaction limit, be $-t$.

Two numerical plots are presented in Fig. 3.2, where exactly the behaviour described above is observed. The singlet-triplet splittings found by the heuristic arguments also match the numerical results. The four-electron system carries much more interesting behaviour, and so we shall turn our attention to it presently.

3.4. Four-electron results

3.4.1. Ferromagnetism of the ground state

As found in Sec. 3.1, the four-electron system exhibits in the translationally invariant non-interacting limit a six-fold degeneracy of the ground state energy $-2t$. As a first approach, we shall again make some heuristic arguments to try to understand the systems limiting behaviour while neglecting for the moment the effects of a magnetic field. Consider $U = 0$ and $\delta/t \ll -1$: two electrons are 'frozen' at $\mathbf{R}_3$, leaving two electrons in the remaining two dots. Effectively, the system is a double-dot filled with two electrons, and this leads to the expectation that the singlet-triplet splitting should approach $-2t$ as in the large detuning limit above. Consider now $U = 0$ and $\delta/t \gg 1$: the system is again effectively a double-dot, but this time it is filled with four electrons. This leads to the immediate conclusion that the ground state must be a singlet, as any triplet is forced to occupy the dot at $\mathbf{R}_3$ with at least one electron.

For $\delta = 0$ and $U/t \gg 1$, we may employ the same argument as in the two-electron case: the local singlet subspace is effectively excluded, leaving the only relevant part of the singlet Hamiltonian for ground state considerations to be $\mathcal{H}^{\text{n-l}}_{N=4}$. Its lowest eigenvalue is $-t + U$, while the lowest eigenvalue of $\mathcal{H}^{S=1}_{N=4}$ is $-2t + U$. In the limit then, the singlet-triplet splitting is t, i.e. the system exhibits ferro-

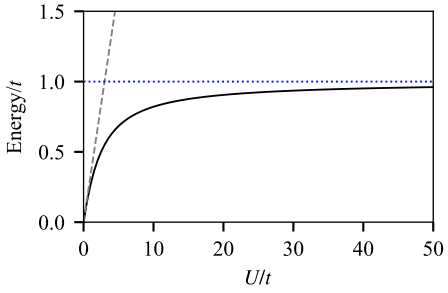

Figure 3.4. The singlet-triplet splitting. The blue dotted line marks an energy of t, and the grey dashed line indicates the first term i the perturbative expansion $\Delta E = U/3$.

magnetism.

This argument is confirmed in Fig. 3.4, which shows by a numerical calculation the singlet-triplet splitting approaching t for $U/t \to \infty$. We would thus expect the ferromagnetism to survive even for finite temperature T if $k_B T \ll t$. The pertinent question now is then for how large detunings at each value of the on-site interaction energy the ferromagnetism is maintained. The next section answers this by presenting a ground state phase diagram.

3.4.2. Phase diagram

A ground state phase diagram is displayed Fig. 3.5, where it is seen that for large parts of the phase space, the system is in fact ferromagnetic. As argued in the above, in the limits $\delta/t \ll -1$ and $\delta/t \gg 1$ the ground state is a singlet, but increasing the on-site interaction energy makes the system ferromagnetic.

The two plots beside the phase diagram are taken along the slices of $U/t = 5$ and $U/t = 15$ as indicated. What can be seen on them is that there in the singlet subspace occurs two crossings, which have been indicated by white dashed lines in the phase diagram. One crossing occurs for all U at $\delta/t = 0$. The other crossing for a given U approaches the line $\delta = U$. To better understand the $\delta = 0$ crossing, we might exactly diagonalise the single-particle Hamiltonian H_{sp} with the detuning. This will break the translational invariance which was taken advantage of in Sec. 3.1. Ignoring spin, the matrix has the following form

$$H_{\text{sp}} = \begin{pmatrix} 0 & -t & -t \\ -t & 0 & -t \\ -t & -t & \delta \end{pmatrix}. \tag{3.27}$$

The mirror symmetry between sites $\mathbf{R}_1$ and $\mathbf{R}_2$ is still present with this detuning, and this mirror symmetry can in the single-particle basis be expressed

$$U_{\text{mir}} = \begin{pmatrix} 0 & 1 & 0 \\ 1 & 0 & 0 \\ 0 & 0 & 1 \end{pmatrix}, \tag{3.28}$$

The fact that $[H_{\text{sp}}, U_{\text{mir}}] = 0$ guarantees simultaneous eigenstates of H_{sp} and U_{mir}, and the latters eigenstates are

$$\begin{aligned} |1\rangle &= \frac{1}{\sqrt{2}}(c_{1\sigma}^\dagger - c_{2\sigma}^\dagger)|\Omega_h\rangle, \\ |2\rangle &= \frac{1}{\sqrt{2}}(c_{1\sigma}^\dagger + c_{2\sigma}^\dagger)|\Omega_h\rangle, \\ |3\rangle &= c_{3\sigma}^\dagger|\Omega\rangle. \end{aligned} \tag{3.29}$$

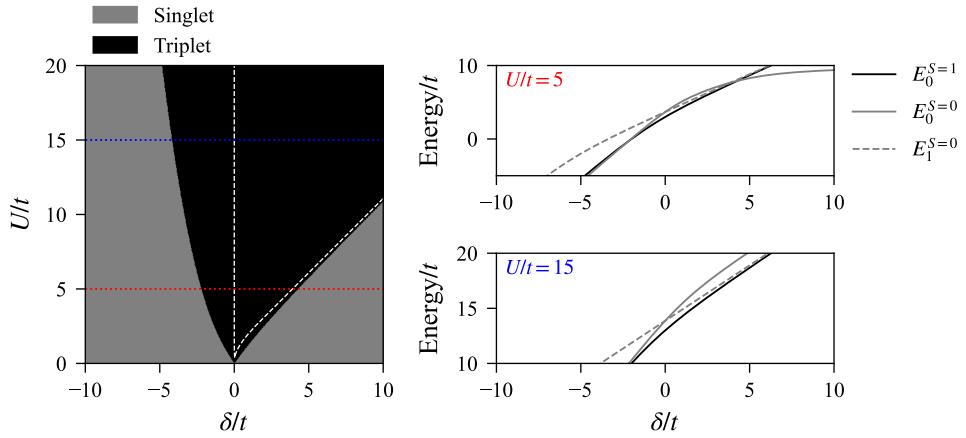

Figure 3.5. Ground state phase diagram and two slices at $U/t = 5$ and $U/t = 15$, which include the lowest triplet energy $E_0^{S=1}$ and the two lowest singlet energies $E_0^{S=0}$ and $E_1^{S=0}$. The plots were produced with $\Phi = 0$.

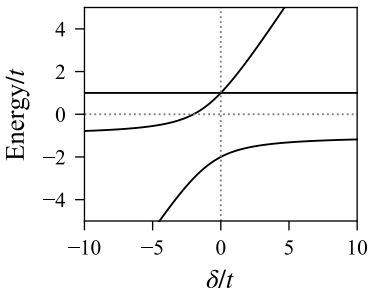

Figure 3.6. The three eigenvalues of H_{sp} with detuning δ.

The similarity matrix $P = (|1\rangle, |2\rangle, |3\rangle)$ will block-diagonalise H_{sp} by the transformation

$$P^{-1} H_{\text{sp}} P = \begin{pmatrix} t & 0 & 0 \\ 0 & -t & -\sqrt{2}t \\ 0 & -\sqrt{2}t & \delta \end{pmatrix}. \tag{3.30}$$

One eigenvalue is t. The other two can easily be found to be

$$\frac{\delta - t}{2} \pm \frac{1}{2}\sqrt{9t^2 + 2t\delta + \delta^2}. \tag{3.31}$$

Plotting all three eigenvalues as a function of δ, as seen in Fig. 3.6, it is clear that when two electrons populate each of the two lowest orbitals, there occurs a crossing at $\delta = 0$. The other crossing is not as straightforward to explain, but the degeneracy occurs close to the line $\delta = U$. The non-local singlets with one electron on the third dot

$$\frac{1}{\sqrt{2}}(c^\dagger_{r,\uparrow} c^\dagger_{r+1,\downarrow} - c^\dagger_{r,\downarrow} c^\dagger_{r+1,\uparrow})|\Omega\rangle \tag{3.32}$$

for $r = 2, 3$ and the local singlet with both electrons removed from the third dot $c_{3\uparrow} c_{3\downarrow} |\Omega_h\rangle$ also experience a crossing in energy exactly at $\delta = U$, which can be seen from their respective matrix elements in Eqs. (3.24) and (3.25). We may therefore infer that it is a kind of local—non-local singlet degeneracy which accounts for the second crossing. Both crossings shall prove to make somewhat more difficult the measurement of the spin and to make necessary the introduction of a second detuning.

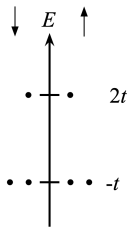

Figure 3.7. Aharonov-Bohm effect at $\Phi/\Phi_0 = 1/2$.

3.4.3. Magnetic effects

As discussed briefly in Sec. 3.1, the Aharonov-Bohm and Zeeman effects affect the spectrum of the system differently—the former splits the crystal momentum degeneracy and the latter splits the spin degeneracy. It is clear to see from Fig. 3.1, that by splitting the crystal momentum degeneracy, the ground state degeneracy between singlets and triplets is also broken, and the ground state favoured by the Aharonov-Bohm effect is then that of the singlet. On the other hand, the Zeeman effect, which energetically favours one spin direction over the other, leads to a triplet ground state. We should then expect in the ground state phase diagram for the parameters Φ and t to see a competition between the two.

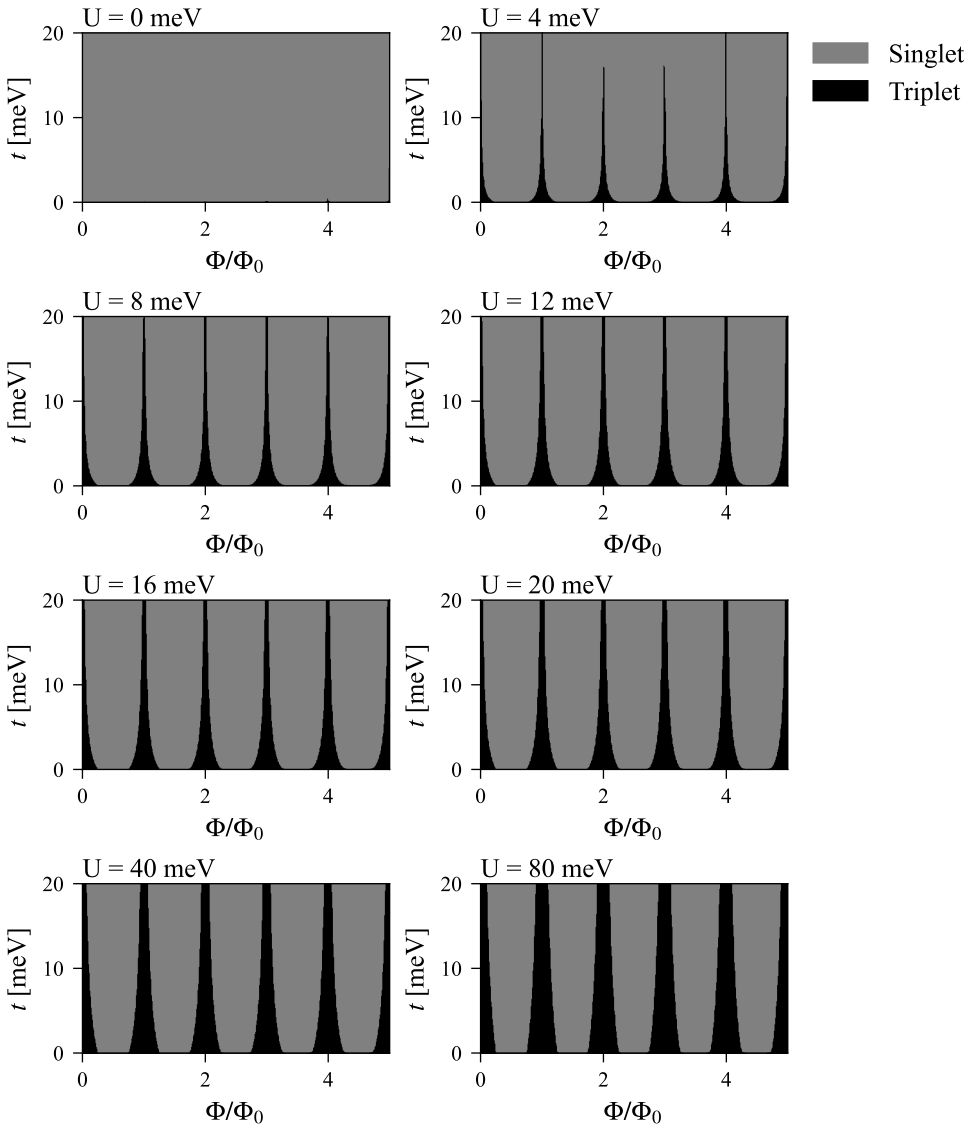

Figure 3.8. Ground state phase diagram for the parameters Φ and t, which show the competition between singlet-preferring Aharonov-Bohm effect and the triplet-preferring Zeeman effect. These plots were produced with $A = (200\,\mathrm{nm})^2/2$ and $g = -0.44$, the latter incidentally resulting in the lowest energy triplet being the one with $S_z = 1$.

In Fig. 3.8, some phase diagrams are presented for different values of U. There is a clear periodicity in the ground state being a singlet or a triplet. When Φ is an integer multiple of Φ_0, the ground state is a triplet, and when Φ is a half-integer multiple of Φ_0, the ground state is a singlet. This can be understood by considering for which values of the flux the spectrum in Fig. 3.1b displays its most extreme configurations. Take $U = 0$ for the moment. When $\Phi = 0$ the singlet and triplet are degenerate, and this behaviour is recovered when $\Phi = \Phi_0$, as can be seen from Eq. (3.6)—the states with crystal momentum k_0 are, so to speak, 'rotated' into the states with crystal momentum k_1, etc., and an identical spectrum is recovered. For Φ between these values, there is a point at $\Phi = \Phi_0/2$ where the singlet-triplet splitting is maximal. At this point the spectrum looks as in Fig. 3.7. This matches exactly the behaviour in the phase diagram.

The relative strength of the Aharonov-Bohm and Zeeman effect is characterised by the ratio $g\mu_B B/t = g\mu_B \Phi/At = -5 \times 10^{-4}$ for $\Phi = \Phi_0$, $A = (200\,\mathrm{nm})^2/2$, $t = 10\,\mathrm{meV}$, and $g = -0.44$, but

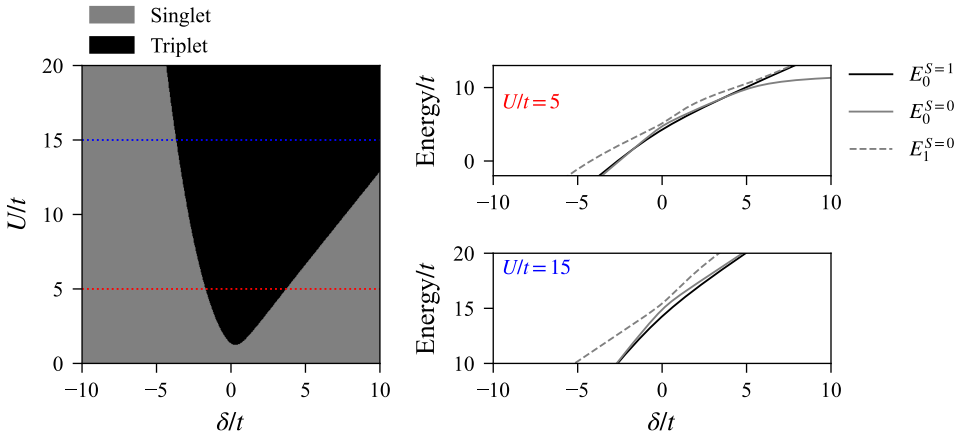

Figure 3.9. Ground state phase diagram and two slices at $U/t = 5$ and $U/t = 15$, which include the lowest triplet energy $E_0^{S=1}$ and the two lowest singlet energies $E_0^{S=0}$ and $E_1^{S=0}$. The plots were produced with $\Phi = 0$ and a second detuning $\delta_2 = t$.

normally attainable magnetic fields are of order 1 T, which for the aforementioned area equates to a flux of about $5\Phi_0$. The small scale of the system is thus the reason that the Zeeman effect is so small as to not be noticable on the scales of the flux presented in the figure. The broadening of the triplet-bands must then also almost exclusively be due to the on-site interaction, which, as explicated in the above sections, favours a triplet ground state. The narrowing of the triplet bands for increasing t is then due to the increase in strength of the Aharonov-Bohm effect in comparison with the on-site interaction, and the Zeeman effect plays no part in this.

3.4.4. Measurement of spin: Introducing a second detuning

If the system is initialised at $\delta = 0$ and a given U, one would like to have a way to measure whether the system is in a triplet or singlet configuration. Increasing δ adiabatically and then measuring the charge on the third dot would be one such way. As δ exceeds a certain threshold, the lowest energy singlet state will have no electrons on the third dot. Meanwhile, the triplet is forced to have one. If the system is initialised into the triplet state, then this is no problem, as δ can indeed be increased adiabatically such that theoretically no state-mixing occurs. However, the singlet measurement is troubled from the very beginning as mentioned in Sec. 3.4.2. As the lowest singlet energy is degenerate at $\delta = 0$, the system will, if initialised as a singlet, be in an unpredictable mix of the two lowest energy singlet states. The second degeneracy close to $\delta = U$, which was theorised to be due to a kind of local—non-local degeneracy, also poses a problem. If δ is adiabatically increased across this crossing, an unpredictable mix of local and non-local singlet states results, which will make any charge measurement ambiguous: the measurement of a charge $-e$ on the third dot could be both a singlet and a triplet, rendering the measurement useless.

In Fig. 3.9 is seen a phase diagram where a second detuning δ_2 on the second dot has been introduced. The translational invariance at $\delta = 0$ is then broken and, as seen in the figure, the second crossing is also eliminated. The splitting between the singlet states at $\delta = 0$ is for $\delta_2 = t$ and $U = 5t$ on the order of $0.4t$. The splitting at the second former crossing is for the same parameter values on the order of $0.7t$. This makes the adiabatic scan possible, and it should be possible to unambiguously distinguish the triplet from the singlet by a charge measurement on the third dot.

3.4.5. Spin-to-charge conversion

We will now relate the spin state to the charge on the third dot. Define the charge operator

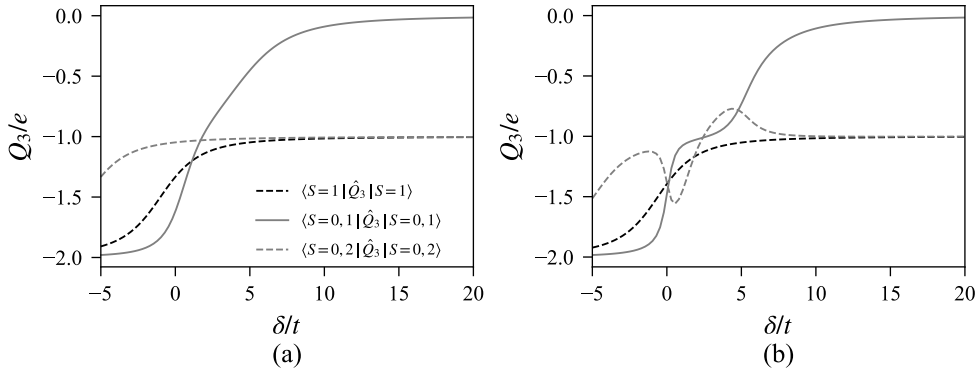

Figure 3.10. The expectation value of $\hat{Q}_3$ in the lowest energy triplet state $|S=1\rangle$ and the two lowest energy singlet states $|S=0,1\rangle$ and $|S=0,2\rangle$. Both plots are produced with $\Phi=0$ and $U/t=5$. In (a), the second detuning $\delta_2=0$. In (b), $\delta_2=t$

$$\hat{Q}_3 = -e\sum_{\sigma} c^{\dagger}_{3,\sigma}c_{3,\sigma} \tag{3.33}$$

Any state $|\psi\rangle$ can be expanded in the basis of the four-electron Hilbert space as

$$|\psi\rangle = \sum_{r,\sigma}\sum_{r',\sigma'}\langle\Omega_h|c^{\dagger}_{r'\sigma'}c^{\dagger}_{r\sigma}|\psi\rangle c_{r,\sigma}c_{r',\sigma'}|\Omega_h\rangle. \tag{3.34}$$

The expansion coefficients $v_{r,r',\sigma,\sigma'} = \langle\Omega_h|c^{\dagger}_{r'\sigma'}c^{\dagger}_{r\sigma}|\psi\rangle$ are the eigenvectors of the Hamiltonian and are found in the numerical exact diagonalisation. The expectation value of $\hat{Q}_3$ can then be written

$$\begin{aligned}\langle\hat{Q}_3\rangle &= \langle\psi|\hat{Q}_3|\psi\rangle \\ &= \sum_{r_1,\sigma_1}\sum_{r_1',\sigma_1'}\sum_{r_2,\sigma_2}\sum_{r_2',\sigma_2'} v^{\dagger}_{r_2,r_2',\sigma_2,\sigma_2'}v_{r_1,r_1',\sigma_1,\sigma_1'}\langle\Omega_h|c^{\dagger}_{r_2,\sigma_2}c^{\dagger}_{r_2',\sigma_2'}\hat{Q}_3 c_{r_1,\sigma_1}c_{r_1',\sigma_1'}|\Omega_h\rangle.\end{aligned} \tag{3.35}$$

As $\hat{Q}_3$ depends only on the number operator $\hat{n}_{3\sigma}$, it is diagonal in the basis. Therefore,

$$\langle\hat{Q}_3\rangle = \sum_{r,\sigma}\sum_{r',\sigma'}\left|v_{r,r',\sigma,\sigma'}\right|^2\langle\Omega_h|c^{\dagger}_{r',\sigma'}c^{\dagger}_{r,\sigma}\hat{Q}_3 c_{r,\sigma}c_{r',\sigma'}|\Omega_h\rangle. \tag{3.36}$$

The representations of $\hat{Q}_3$ in the four-electron Hilbert space basis is for the three triplet subspaces

$$Q_3^{S=1} = \mathrm{diag}(-2e,-e,-e), \tag{3.37}$$

and for the singlet subspace

$$Q_3^{S=0} = \mathrm{diag}(-2e,-2e,0,-2e,-e,-e). \tag{3.38}$$

In Fig. 3.10, two plots of $\langle\hat{Q}_3\rangle$ are presented. One for $\delta_2=0$ and one for $\delta_2=0.1t$. We see that in the lowest-energy singlet state, the charge on the third dot vanishes, while for the second-lowest singlet state, it approaches $-e$, and it is therefore a non-local singlet state as theorised. Thus, adding a second small detuning parameter δ_2 should make discriminating between singlets and triplets by adiabatically increasing the detuning to or above $\delta\sim 5t$ possible.

Chapter 4

Conclusion

In this thesis, the magnetic properties of a toy model of a three-site quantum dot system with a triangular geometry has been explored. A negative result is obtained, when the system is populated with two electrons. In this case, no parts of the phase space exhibit ferromagnetism, and the singlet-triplet splitting is generally bigger than or equal to $-2t$. Conversely, four-electron filling of the system results in large parts of the phase space of the system being ferromagnetic, as seen in Fig. 3.5, with the singlet-triplet splitting approaching the hopping parameter t in the large on-site interaction limit. Thus, for thermal energies $k_B T \ll t$, one should in experiments expect to observe ferromagnetism in the system. The Aharonov-Bohm effect was in addition found to be more important than the Zeeman effect due to the small size of the system.

A protocol for measurement of the spin of the ground state was proposed based on adiabatically increasing the detuning parameter from $\delta = 0$ to $\delta \sim 5t$ or above, as this introduces a charge difference between the singlet and the triplet of one elementary charge $-e$. Introduction of a secondary small detuning parameter δ_2 is necessary for this procedure, as it breaks the degeneracies in the singlet subspace and therefore allows the adiabatic increase of the detuning parameter without unpredictable state mixing within the singlet subspace.

Further theoretical work on this system could include the inclusion in the model of further effects, such as the Rashba spin-orbit coupling or calculations for less symmetric configurations of the systems, i.e. non-homogeneous U_r or t_r.

Bibliography

[1] Daniel P. Arovas et al. “The Hubbard Model”. In: *Annual Review of Condensed Matter Physics* 13.1 (2022), pp. 239–274. DOI: 10.1146/annurev-conmatphys-031620-102024. URL: https://doi.org/10.1146%2Fannurev-conmatphys-031620-102024.

[2] Henrik Bruus and Karsten Flensberg. *Many-body quantum theory in condensed matter physics*. Oxford Graduate Texts. Oxford University Press, 2004. ISBN: 9780198566335.

[3] J. P. Dehollain et al. “Nagaoka ferromagnetism observed in a quantum dot plaquette”. In: *Nature* 579.7800 (2020), pp. 528–533. DOI: 10.1038/s41586-020-2051-0. URL: https://doi.org/10.1038%2Fs41586-020-2051-0.

[4] David J. Griffiths and Darrell F. Schroeter. *Introduction to Quantum Mechanics*. 3rd ed. Cambridge University Press, 2018. ISBN: 9781107189638.

[5] Panagiotis Kotetes. *Topological Insulators*. IOP Concise Physics. Bristol, UK: Morgan & Claypool Publishers, 2019. ISBN: 9781681745176.

[6] Daniel Loss and David P. DiVincenzo. “Quantum computation with quantum dots”. In: *Phys. Rev. A* 57 (1 1998), pp. 120–126. DOI: 10.1103/PhysRevA.57.120. URL: https://link.aps.org/doi/10.1103/PhysRevA.57.120.

[7] Yosuke Nagaoka. “Ferromagnetism in a Narrow, Almost Half-Filled *s* Band”. In: *Phys. Rev.* 147 (1 1966), pp. 392–405. DOI: 10.1103/PhysRev.147.392. URL: https://link.aps.org/doi/10.1103/PhysRev.147.392.

[8] Steven H Simon. *The Oxford solid state basics*. Oxford, UK: Oxford Univ. Press, 2013. ISBN: 0199680760.

[9] Claude Weisbuch and Claudine Hermann. “Optical detection of conduction-electron spin resonance in GaAs, $Ga_{1-x}In_xAs$, and $Ga_{1-x}Al_xAs$”. eng. In: *Physical review. B, Solid state* 15.2 (1977), pp. 816–822. ISSN: 0556-2805.

Appendix A

Second quantisation

This appendix is a brief introduction to second quantisation. Treating many-electron systems in the first quantisation formalism of quantum mechanics, as expounded in Griffiths [4], requires complicated antisymmetrisation procedures due to the indistinguishability of electrons.[1] The wavefunction of an N-electron system $\Psi(\mathbf{r}_1, \mathbf{r}_2, \ldots, \mathbf{r}_N)$ is the position representation of a state vector $|\Psi\rangle$, an element of the antisymmetric subspace of an N-particle Hilbert space, which may be denoted $A\mathscr{H}^{\otimes N}$. The appropriate position space basis is composed of the Slater determinants, which are functions of the form $B\hat{A}\prod_{i=1}^{N}\psi_{\nu_i}(\mathbf{r}_i)$, where $\{\psi_\nu(\mathbf{r})\}$ is an ordered orthonormal position basis of the single-particle Hilbert space characterised by set of quantum numbers $\{\nu\}$, B is a normalisation factor, and $\hat{A}$ is the antisymmetriser: an operator which superposes the product states such that interchange of any two different coordinates $\mathbf{r}_j$ and $\mathbf{r}_k$ leads to a sign change of the wavefunction. Operators in first quantisation also depend upon the number of particles under consideration.

Second quantisation is a signficantly simpler formalism for dealing with many-electron systems. Assuming as before an ordered orthonormal basis for the single-particle Hilbert space $\{|\nu_i\rangle\}$ for $i = 1, 2, \ldots$, we label states simply by the occupation number n_{ν_j} of each orbital $|\nu_j\rangle$,

$$|\Psi\rangle = |n_{\nu_1}, n_{\nu_2}, \ldots\rangle; \qquad \sum_i n_{\nu_i} = N. \tag{A.1}$$

Of course for electrons, only $n_{\nu_j} = 0, 1$ is possible due the Pauli exclusion principle. The latter equation above restricts the states to the same Hilbert space $A\mathscr{H}^{\otimes N}$ discussed above. If it is relaxed, the states span a more general space called the Fock space $\mathscr{F}$, which encompasses states of all possible particle numbers.

Handling these states is done by defining the operator c_{ν_j} and its Hermitian conjugate $c^\dagger_{\nu_j}$, which are said respectively to annihilate and create a particle in the orbital $|\nu_j\rangle$. They are defined by their action on the state vector

$$\begin{aligned} c^\dagger_{\nu_j}|\ldots, n_{\nu_j}, \ldots\rangle &= |\ldots, n_{\nu_j} + 1, \ldots\rangle, \\ c_{\nu_j}|\ldots, n_{\nu_j}, \ldots\rangle &= |\ldots, n_{\nu_j} - 1, \ldots\rangle. \end{aligned} \tag{A.2}$$

This definition and the required sign change of the state vector upon interchange of any two particle labels leads to an operator algebra defined by the following anticommutation relations:

$$\{c_{\nu_i}, c_{\nu_j}\} = 0, \qquad \{c^\dagger_{\nu_i}, c^\dagger_{\nu_j}\} = 0, \qquad \{c^\dagger_{\nu_i}, c_{\nu_j}\} = \delta_{\nu_i,\nu_j}, \tag{A.3}$$

where $\{A, B\} = AB - BA$ is the anticommutator of A and B. Thus, an N-particle state may be constructed by operating on the vacuum state $|\Omega\rangle = |0, 0, \ldots\rangle$ with creation operators, which yields

$$|\Psi\rangle = \prod_{i=1}^{N} c^\dagger_{\nu_i}|\Omega\rangle. \tag{A.4}$$

[1] This appendix is based on Chapter 1 in [2].

The most important operators in this formalism are the particle number operator $\hat{n}_{\nu_j} = c^\dagger_{\nu_j} c_{\nu_j}$ and the total particle number operator $\hat{N} = \sum_i c^\dagger_{\nu_i} c_{\nu_i}$. Operating on a state $|\Psi\rangle$ as defined in the above equation gives

$$\hat{n}_{\nu_j}|\Psi\rangle = n_{\nu_j}|\Psi\rangle; \qquad \hat{N}|\Psi\rangle = N|\Psi\rangle. \tag{A.5}$$

In fact, in second quantisation, all operators can be expressed as linear combinations of products of annihilation and creation operators, and they do not depend on the particle number.

Specialising to the triple QD-system described in Chapter 1, we have $\{\nu\} = \{(r, \sigma)\}$ as the basis is $\{|\psi_r\rangle \otimes |\sigma\rangle\}$. This leads naturally to the creation and annihilation operators $c^\dagger_{r,\sigma}$ and $c_{r,\sigma}$ interpreted as respectively creating or annihilating an electron in the state $|\psi_r\rangle \otimes |\sigma\rangle$. As a notational shorthand $c_{r,\uparrow}$ and $c_{r,\downarrow}$ (equivalently for the creation operators) can be collected in the spinor $c_r = (c_{r,\uparrow}, c_{r,\downarrow})^T$, which transforms under SU(2).

Appendix B

Conservation of spin

This appendix contains some results which are used in Sec. 2.3.2.

It was claimed that if the Hamiltonian commutes with the unitary operators $\Theta_{\boldsymbol{\alpha}}$ representing spin rotations, then it commuted with the spin operators. This follows from considering the object

$$\begin{aligned}\frac{\mathrm{d}}{\mathrm{d}s}[\mathcal{H}, e^{si\mathbf{S}\cdot\boldsymbol{\alpha}}] &= \mathcal{H}(i\mathbf{S}\cdot\boldsymbol{\alpha})e^{si\mathbf{S}\cdot\boldsymbol{\alpha}} - (i\mathbf{S}\cdot\boldsymbol{\alpha})e^{si\mathbf{S}\cdot\boldsymbol{\alpha}}\mathcal{H} \\ &= [\mathcal{H}, i\mathbf{S}\cdot\boldsymbol{\alpha}]e^{si\mathbf{S}\cdot\boldsymbol{\alpha}}. \end{aligned} \tag{B.1}$$

If $[\mathcal{H}, \Theta_{\boldsymbol{\alpha}}] = 0$ for all $\boldsymbol{\alpha}$ is assumed to hold, then the left-hand side of the above equation must vanish, i.e. $(\mathrm{d}/\mathrm{d}s)[\mathcal{H}, e^{si\mathbf{S}\cdot\boldsymbol{\alpha}}] = 0$. The consequence of this is that $[\mathcal{H}, \hat{S}_i] = 0$ for all i.

We now prove the relation in Eq. (2.30). Assume $\boldsymbol{\alpha}$ to be parallel with one of the axes $i = x, y, z$. We use a lemma of the Baker-Campbell-Hausdorff formula to get

$$\begin{aligned}\Theta_{\boldsymbol{\alpha}} c_r \Theta_{\boldsymbol{\alpha}}^\dagger &= e^{i\alpha S_i} c_r e^{-i\alpha S_i} \\ &= c_r + [i\alpha S_i, c_r] + \frac{1}{2!}[i\alpha S_i, [i\alpha S_i, c_r]] + \cdots \\ &= c_r + \frac{i\alpha}{2}[c_r^\dagger \sigma_i c_r, c_r] + \frac{1}{2!}\Big(\frac{i\alpha}{2}\Big)^2 [c_r^\dagger \sigma_i c_r, [c_r^\dagger \sigma_i c_r, c_r]] + \cdots \end{aligned} \tag{B.2}$$

The first commutator is

$$\begin{aligned}[c_r^\dagger \sigma_i c_r, c_r] &= c_r^\dagger \sigma_i c_r c_r - c_r c_r^\dagger \sigma_i c_r \\ &= -\sigma_i c_r, \end{aligned} \tag{B.3}$$

due to the first term vanishing upon application to any state, and the anticommutation relations. The next commutator is

$$\begin{aligned}[c_r^\dagger \sigma_i c_r, [c_r^\dagger \sigma_i c_r, c_r]] &= -[c_r^\dagger \sigma_i c_r, \sigma_i c_r] \\ &= -c_r^\dagger \sigma_i c_r \sigma_i c_r + \sigma_i c_r c_r^\dagger \sigma_i c_r \\ &= \sigma_i^2 c_r - \sigma_i c_r^\dagger c_r \sigma_i c_r \\ &= c_r. \end{aligned} \tag{B.4}$$

It is clear that the nested commutators have a cyclic structure, which allows writing the expression as

$$\begin{aligned}\Theta_{\boldsymbol{\alpha}} c_r \Theta_{\boldsymbol{\alpha}}^\dagger &= c_r - \frac{i\alpha}{2}\sigma_i c_r + \frac{1}{2!}\Big(\frac{i\alpha}{2}\Big)^2 c_r - \frac{1}{3!}\Big(\frac{i\alpha}{2}\Big)^3 \sigma_i c_r + \cdots \\ &= \Big[1 - \frac{1}{2!}\Big(\frac{\alpha}{2}\Big)^2 + \cdots\Big] c_r - i\Big[\frac{\alpha}{2} - \frac{1}{3!}\Big(\frac{\alpha}{2}\Big)^3 + \cdots\Big]\sigma_i c_r \\ &= \cos\Big(\frac{\alpha}{2}\Big) - i\sin\Big(\frac{\alpha}{2}\Big)\sigma_i c_r \end{aligned}$$

$$= e^{-i\alpha\sigma_i/2} c_r \tag{B.5}$$

Letting $U = e^{-i\alpha\sigma_i/2}$ and noting that the Pauli matrices are Hermitian, we see that $UU^\dagger = e^{-i\alpha\sigma_i/2} e^{i\alpha\sigma_i/2} = 1$, confirming that $U \in \mathrm{SU}(2)$.